J. Fluid Mech. (1983), *vol.* 133, *pp.* 377–395
Printed in Great Britain

The growth of a grid-generated turbulent mixed layer in a two-fluid system

By HARINDRA J. S. FERNANDO AND ROBERT R. LONG

Department of Earth and Planetary Sciences, The Johns Hopkins University, Baltimore, Maryland 21218

(Received 20 December 1982 and in revised form 19 April 1983)

This paper describes a laboratory experiment designed to compare measurements with published theoretical ideas of the mixed-layer growth of a two-layer system in which the turbulence is induced by an oscillating grid. Experimental results show excellent agreement with an earlier theory by one of us (Long), in which the mixed-layer depth D_* measured from a virtual origin is given by $D_* \sim V_0^{-\frac{7}{11}} K^{\frac{8}{11}} t^{\frac{9}{11}}$, where K is action, t is time and V_0 is a characteristic velocity of the problem. The experiments also verify Long's theoretical entrainment relation $E = \alpha_2 Ri^{-\frac{1}{4}}$, where E is the entrainment coefficient and $Ri = D_*^3 \Delta b / K^2$, and Δb is the buoyancy difference between the two layers. The interfacial-layer thickness was observed to be proportional to the depth of the mixed layer, as also predicted by Long. After a certain depth, the entrainment law tends to deviate from Long's theory. The deviation may be due to wall effects.

1. Introduction

Turbulent mixing in a stably stratified fluid has attracted great interest from fluid-dynamicists because of its importance in various phenomena in geophysics and engineering. The roots of its study can be found as far back as the classical work of Ekman (1905), but the first experiments on mixing were run by Rouse & Dodu (1955). They used two initially homogeneous layers with an oscillating grid agitating the upper layer. They kept the interfacial layer at the same position by allowing water to flow into the lower layer and out of the upper mixed layer. A similar experiment of a qualitative nature for the linearly stratified case was conducted by Cromwell (1960).

In the geophysical context, the experiments performed to date fall into four broad categories: (*a*) oscillating-grid experiments (Bouvard & Dumas 1967; Turner 1968; Wolanski 1972; Crapper & Linden 1974; Thompson & Turner 1975; Linden 1975; Wolanski & Brush 1975; Hopfinger & Toly 1976; McDougall 1979; Folse, Cox & Schexnayder 1981; Ivey & Corcos 1982); (*b*) shear-driven experiments to simulate mixing due to drift currents (Ellison & Turner 1959; Loftquist 1960; Kato & Phillips 1969; Wu 1973; Kantha, Phillips & Azad 1977; Deardorff & Willis 1982; Scranton & Lindberg 1982); (*c*) convective stirring experiments to simulate the mixing due to seasonal and diurnal heating and cooling (Deardorff, Willis & Lilly 1969; Deadorff, Willis & Stockton 1980; Long & Kantha 1979); (*d*) experiments designed in an attempt to understand turbulent mixing in a stably stratified fluid under an imposed stabilizing buoyancy flux (Turner & Kraus 1967; Moore & Long 1971; Kantha & Long 1980; Hopfinger & Linden 1982). Additional references for the four categories can be found in Turner (1973), Phillips (1976) and Kitaigorodskii (1979).

Aside from its geophysical implications, turbulent mixing is also important in studies of water-quality control in the hypolimnion in stratified reservoirs (Fisher *et al.* 1979), pollution in the atmosphere and various bodies of water (Baines 1975), studies of the spreading angle in supersonic jets (Brown & Roshko 1974), problems of the control of the water temperature in multi-outlet water reservoirs (e.g. Oroville reservoir, Fisher *et al.* 1979) the design of solar ponds to obtain maximum temperatures (Leshuk *et al.* 1978), etc.

Although the large number of contributions has improved our understanding of mixed-layer dynamics in many respects, more theoretical work is necessary. As we would expect, closure of the dynamical equations becomes even more difficult in the presence of stratification. In this connection, Rouse & Dodu (1955) argued that the rate of change of potential energy is proportional to the input of kinetic energy, so that the entrainment coefficient ($E = u_e/u_*$, where u_e is the entrainment rate defined as $\mathrm{d}D/\mathrm{d}t$, D is the depth of the mixed layer and u_* is a scaling velocity) is inversely proportional to the Richardson number $Ri_1 = D\Delta b/u_*^2$, where Δb is the buoyancy jump across the interface. This seems not to predict the results of the grid experiments, but some support for this law can be seen in the shear experiments of Kato & Phillips (1969) and Moore & Long (1971).

Following a valuable idea by Turner (1973) that quantities near the interface are the ones that are dynamically important for entrainment, Linden (1975) suggested that the rate of change of potential energy of the stratified system is proportional to the kinetic energy available at the interface. Although the resulting prediction of the time dependence of the mixed-layer depth shows a possible agreement with observations, close inspection reveals disagreements (Folse *et al.* 1981).

A model of the grid as a source of turbulence has been constructed by Long (1978*a*), who derived a single parameter of the dimensions of eddy viscosity called grid 'action' K, characteristic of the grid and its motion. Long (1978*a*) showed that at high Reynolds numbers the r.m.s. velocity σ_u and the integral lengthscale l, measured at a distance z from a virtual origin, become

$$\sigma_u \sim \frac{K}{z}, \tag{1}$$

$$l \sim z. \tag{2}$$

Based partly on measurements and on dimensional arguments, Thompson & Turner (1975) and Hopfinger & Toly (1976) proposed

$$\sigma_u = C_1 S^{\frac{5}{2}} \omega z^{-\frac{3}{2}}, \tag{3}$$

$$\sigma_u = C_2 S^{\frac{3}{2}} M^{\frac{1}{2}} \omega z^{-1} \tag{4}$$

respectively, where S is the stroke, M is the mesh size, ω is the frequency of the grid oscillation, and C_1, C_2 are constants.

'Action' can be evaluated in two ways: (i) by observing the deepening of the mixed layer in a homogeneous fluid and using $D_* = (Kt)^{\frac{1}{2}}$, where D_* is the thickness of the mixed layer measured from a virtual origin (Dickinson & Long 1978, 1983), and (ii) using $K_l = \sigma_u l$ (Long 1978*b*). These differ by a numerical factor ($K = 7K_l$). Additional experimental support for the concept of 'action' is found in Dickinson & Long (1983), Thompson (1969), McDougall (1979), Hopfinger & Toly (1976), Folse *et al.* (1981). In particular, McDougall (1979) has found it unfortunate that the $z^{-\frac{3}{2}}$ relation has been widely used, but for our present purposes we will continue to entertain this relation as a possibility.

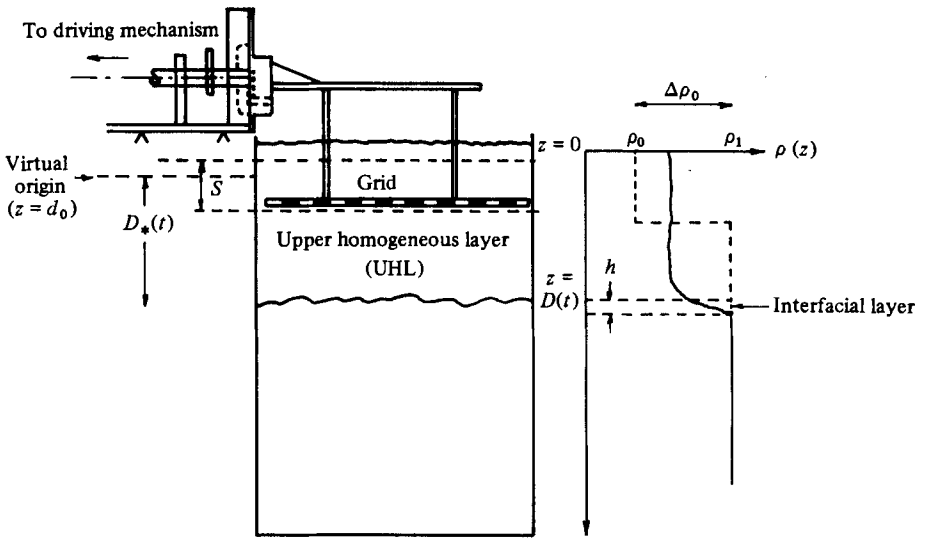

FIGURE 1. Schematic view of experimental apparatus.

We believe that the results of oscillating-grid experiments may be applicable to mixing due to wave-breaking in the oceans, tidal mixing in a stratified channel, mixing in a fjord due to periodically changing winds, etc. Also, grid mixing is apparently one of the simpler examples of turbulence, and is one for which there are detailed theories (Long 1978*a*, *b*). Therefore we have undertaken in this paper to investigate in detail the influence of various parameters on the deepening of the mixed layer in a two-fluid system in order to check the hypotheses presented so far in the literature relevant to this process.

2. Analytical considerations

For the given configuration in figure 1 (but neglecting the thickness of the interfacial layer), the potential energy per unit area can be written (Linden 1975)

$$A = \tfrac{1}{2}\rho_1 D D_0 \Delta b_0 + \text{const} = \tfrac{1}{2}\rho_1 V_0^2 D + \text{const}, \tag{5}$$

where D_0 is the initial depth of the upper layer, Δb_0 is the buoyancy jump across the interface at an arbitrary time t_0, and ρ_1 is the reference density (density in the lower, undisturbed layer). From continuity, $D\Delta b = D_0 \Delta b_0 = V_0^2$ is constant. If the depth of the mixed layer measured from a virtual origin located at a distance d_0 from the top of the layer (figure 1) is D_*, the rate of change of potential energy becomes

$$\frac{\mathrm{d}A}{\mathrm{d}t} = \tfrac{1}{2}\rho_1 V_0^2 \dot{D}_*, \tag{6}$$

where the dot represents differentiation with respect to time. Let us now obtain the dependence on time of the mixed-layer depth in two ways using the hypotheses of Rouse & Dodu (1955) and Linden (1975).

(*a*) If the rate of change of potential energy of the system, proportional to $\mathrm{d}D_*/\mathrm{d}t$, is a constant fraction of the energy flux by the grid (Rouse & Dodu 1955) (i.e. proportional to $\omega^3 S^3$), the entrainment law becomes

$$D = C_3 V_0^{-2} S^3 \omega^3 t, \tag{7}$$

where C_3 is a universal constant.

(*b*) If the rate of change of potential energy is proportional to the kinetic energy available at the interface (i.e. σ_u^3), it is possible to apply the argument of Linden (1975) for his linearly stratified model to the two-layer case in a simple manner. Using (6), together with (3) and (4), we obtain respectively

$$D_* = C_4 V_0^{-\frac{4}{11}} \omega^{\frac{6}{11}} S^{\frac{15}{11}} t^{\frac{2}{11}} \quad (\sigma_u \sim z^{-\frac{3}{2}}), \tag{8}$$

$$D_* = C_5 V_0^{-\frac{1}{2}} \omega^{\frac{3}{4}} S^{\frac{6}{5}} M^{\frac{3}{8}} t^{\frac{1}{4}} \quad (\sigma_u \sim z^{-1}), \tag{9}$$

where C_4 and C_5 are universal constants.

On the other hand, Long (1978*b*) has offered several arguments pertaining to the problem of entrainment in order to close the set of equations consisting of the energy equation and the integrated buoyancy equation across the mixed layer and the interfacial layer. They include the following:

(i) The interfacial layer is continuously agitated by the eddies in the mixed layer. The large eddies move over the interface and become distorted (flattened) as in motion over a rigid surface. During this motion, there is an exchange of energy from the vertical to the horizontal component of velocity in accordance with the theory of Hunt & Graham (1978). This was verified later by McDougall (1979) and Piat & Hopfinger (1981). Further, these large-scale, flattened eddies do not possess enough kinetic energy (vertical component) to cause entrainment, so that the quasi-isotropic eddies contained in the energy spectra at the same levels, which do not feel the presence of the interface, are responsible for the entrainment. These quasi-isotropic eddies have an energy distribution which follows Kolmogorov's $k^{-\frac{5}{3}}$ relation.

(ii) In the interfacial layer, the kinetic energy of turbulence and available potential energy of the eddies are of the same order, and this contributes to the determination of the thickness of the turbulent patches formed due to breaking of interfacial waves at the top of the interfacial layer. Turbulence in the interfacial layer is intermittent, and the intensity of turbulence decreases as distance from the mixed layer increases. In this layer the dissipation, energy-flux divergence and buoyancy flux are all of the same order.

(iii) Entrainment occurs (i.e. buoyancy flux exists) owing to the breaking of internal waves in the interfacial layer. This wave-breaking occurs through a resonance mechanism in which the forcing is accomplished by the eddies of the mixed layer acting on the upper surface of the interfacial layer.

(iv) Dissipation varies vertically within the interfacial layer. Near the mixed-layer/interfacial-layer boundary, dissipation is attributable to a cascade process in which energy flows from large eddies of the size of the mixed-layer depth D_* to the small, quasi-isotropic eddies. As the distance downward from the mixed-layer/interfacial-layer boundary increases, the dissipating eddies of the small Kolmogorov scales receive energy from the large eddies of the size of the turbulent patches through a cascade mechanism. Also in this case, the dissipation is a function of the depth of the mixed layer D_* and the distance from the interfacial-layer/mixed-layer boundary.

Using these arguments, Long (1978*b*) finds for the two-layer case

$$D_* = B_8 V_0^{-\frac{7}{11}} K^{\frac{8}{11}} t^{\frac{2}{11}}, \tag{10}$$

$$h = \alpha_1 D_*, \tag{11}$$

$$E = \frac{u_e}{K/D_*} = \alpha_2 Ri^{-\frac{7}{4}}, \tag{12}$$

where u_e is the entrainment velocity, $Ri = D_*^3 \Delta b / K^2$ is the Richardson number, h

is the interfacial-layer thickness, and α_1, α_2 and B_8 are universal constants. Note that the agreement of the exponent of t in (8) and (10) is fortuitous, and a comparison with experiment requires an investigation also of the dependency of D_* on V_0 and K in (10) and, because S is constant (for the present experiment), on ω and V_0 in (8).

3. The experiment

The experimental tank is a 22.5 in. × 22.5 in. × 24 in. Plexiglas container. A horizontal grid, which has a sliding fit with the container and is free to oscillate in a vertical plane, is held in the upper portion of the tank by three connecting bars of $\frac{1}{4}$ in. diameter, which in turn are connected to the slider of the oscillating mechanism. Rotary motion of the motor is converted to the reciprocating motion of the slider by a mechanism which was a part of an American optical microtome, finished precisely to give a sinusoidal motion by a slider-crank-type mechanism. The amplitude of the vertical oscillations (which is defined as half the stroke length S) is 2.5 cm (figure 1). The mechanism is powered by a $\frac{1}{2}$ horsepower electric motor via a reduction gearbox and a flexible coupling. The frequency was varied by a speed controller. The frequencies used (viz 8–14 rad/s) were, we hope, low enough to prevent the unwanted mean circulations reported by McDougall (1979). The 'action' of the grid used in the experiment has been calibrated with respect to frequency ω by Dickinson (1980) (see also Dickinson & Long 1983) by observing the growth of a turbulent layer in a homogeneous fluid and comparing with the equation $D_* = (Kt)^{\frac{1}{2}}$. The result is contained in figure 2. The grid consists of square Plexiglas bars of cross-section $\frac{3}{8}$ in. × $\frac{3}{8}$ in., aligned in a square array with 1.875 in. between the centres of the bars. The geometric solidity of the grid is 36 % and, in the present case, should not differ very much from the fluid-mechanical solidity (Corrsin 1963).

We should mention another important factor concerning grid-generated turbulence, namely the 'unstable jet-switching phenomenon'. According to Corrsin (1963), '...the wake system will be unstable in the large when the fraction of duct area blocked is sufficiently great. Then the individual jets coalesce successively into larger and larger jets by actual gross direction changes. The resulting turbulence is not only of larger scale and more intense than in the stable case but is less likely to be homogeneous.' This multiple jet-switching phenomenon is more pronounced at such high solidities as 60 %.

In setting up the experiment, a known amount of fresh water coloured with sodium florescein dye was put in the tank. Salt water was then allowed to flow into the bottom of the tank very slowly in order to avoid mixing. The position of the top of the upper layer was always held at a fixed position relative to the grid. Experiments were begun by simultaneously starting the motor and the electronic timer. Deepening of the mixed layer was monitored and verified by the observations on a shadowgraph. A horizontal laser beam was traversed vertically to estimate the interfacial-layer thickness by a method described by Thorpe (1973). In addition, a vertical sheet of laser light was passed through the tank and the resulting image was observed on the shadowgraph. When the laser beam was properly located (the laser was mounted on a frame and was free to move in a vertical plane), the latter technique gave a much clearer estimate of the interfacial-layer thickness. A single-electrode conductivity probe was traversed vertically over the total depth of the tank, and the recordings of depth *vs.* density data were plotted on an (x, y)-recorder. Additional observations were made by a fixed conductivity probe giving conductivity variations at a point with respect to time. Depth/conductivity plots were also used to estimate the

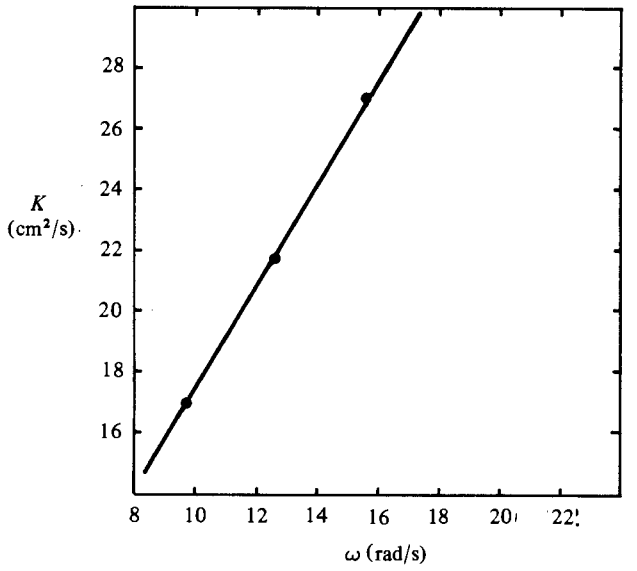

FIGURE 2. Action/frequency behaviour of the grid of Dickinson & Long (1983).

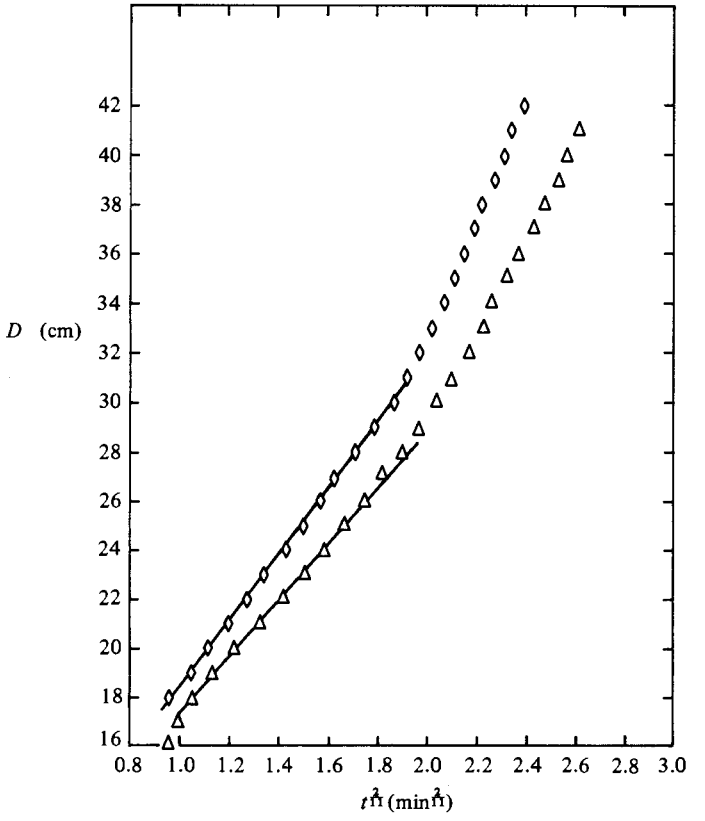

FIGURE 3. Graph of D *vs.* $t^{\frac{1}{2}}$ for two experiments: ◇, $V_0 = 12.03$ cm/s, $K = 18.7$ cm²/s; △, $V_0 = 15.24$ cm/s, $K = 18.7$ cm²/s.

interfacial-layer thickness according to a method described in detail by Crapper & Linden (1974).

The depth D of the mixed layer was plotted against $t^{\frac{3}{4}}$ as seen for example in figure 3. In each such plot a linear relation is seen at the smaller depths, followed at a certain point ('breakpoint') by another linear relation with increased slope (increased entrainment rate). The fit of these data (up to the breakpoint) to the curve $D = \alpha t^{\frac{3}{4}} + d_0$ was accomplished by a last-square computer program, and the distance d_0 from the virtual origin to the free surface and the slope α of the graph were found. Both correlation coefficient and standard error were used in determining the breakpoint, and hence the number of readings included in calculating the slope. Close observation of the location of the virtual origin revealed that in most experiments it lay between 6.0–7.5 cm below the free surface whereas the mean grid position was 6.75 cm (i.e. the virtual origin was in a thin strip about the midplane of the grid). This small variaion of d_0 seemed to have no relation to the size of V_0 or K. Hopfinger & Toly (1976) have observed the position of the virtual origin (which they define as the point with zero integral lengthscale) at a distance of $(\frac{1}{2}S + 1$ cm$) \pm 0.5$ cm from the top position of the grid.

Errors in the final results were estimated using the method devised by Kline & McClintock (1953) in which final uncertainty is estimated from the uncertainty of each independent measurement. For the present experiments, the uncertainties were ± 0.2 cm for D, ± 2 s for t, and ± 4.9 cm/s^2 for Δb, so that the calculated maximum possible uncertainties were ± 0.233 cm/min$^{\frac{3}{4}}$ for the slope α, ± 3 cm/s for V_0, and ± 1.25 cm^2/s for K.

4. Qualitative observations

During the initial period of deepening, the wake and jet structure produced near the grid could easily be seen. A conductivity probe held near the midplane of the grid and 5 cm below the midplane revealed forced salinity fluctuations at these points with the same frequency as that of the grid. The effect could not be observed at a distance of about twice the stroke length, and hence the data taken near the grid were omitted from final calculations. After the initial period of deepening, the interface descends regularly. Shadowgraph observation clearly shows travelling internal waves on the interfacial layer. Observations on a shadowgraph by a thin vertical sheet of laser light were most striking, and showed both the highly active upper part of the interfacial layer and less active lower part. Also a laser beam passing through the interface bends appreciably indicating the high density gradients. In a strip at the top of the interfacial layer the curvature of the density profile was seen to be a maximum, and the thickness of this strip reduces as the interface descends. Internal waves generated on the upper part, while travelling, steepen and break by bursting at the 'tips' of the waves. Careful observations also show that, once the internal wave breaks, the tip rises and mixes with the upper layer rather than advecting horizontally. Figure 4 shows a time-series record on an (x, y)-plotter of salinity fluctuations at a fixed point which is initially in the interfacial layer. The record shows that fluctuations are much larger in the interfacial layer than in the mixed layer. As time increases, the interface descends and, when the bottom of the mixed layer coincides with the probe position, vigorous fluctuations can be seen. Further observations of salinity fluctuations at various points in the interfacial layer show a somewhat decreased activity as the interfacial layer moves away from the grid. Time-series observations also clearly show a decreased intensity at the top of the interfacial layer as the distance from the grid

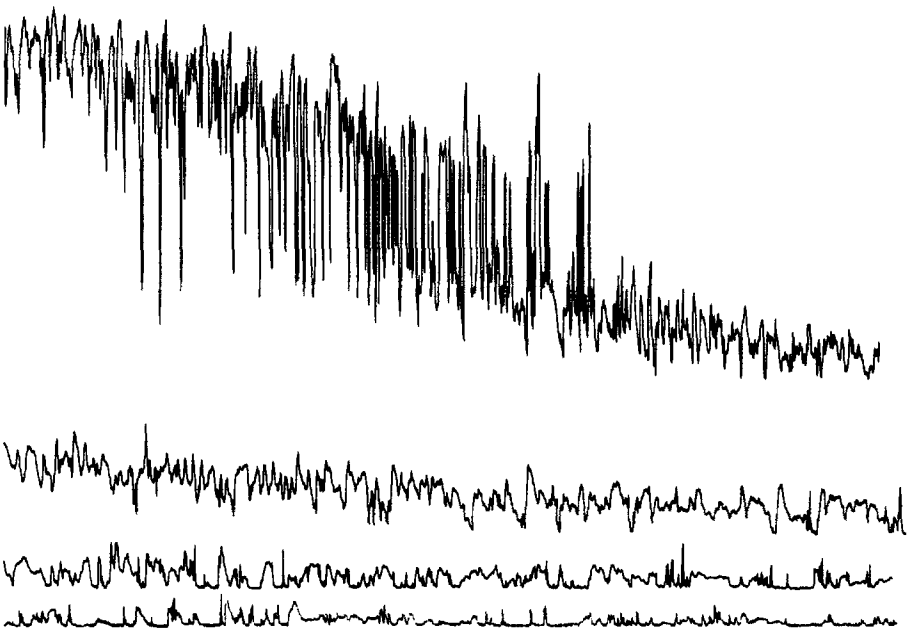

FIGURE 4. Time-series conductivity fluctuations recorded by a fixed conductivity probe. Initially the probe was in the interfacial layer. (Horizontal scale: one inch represents 100 s).

increases. Another event, observed most frequently at small values of D (low Ri), is the splashing out of fluid in the interfacial layer by large-scale eddies burying themselves in it. Linden (1973) has suggested this as a possible entrainment mechanism at low Richardson number, by which he may mean that the splashed-out fluid retreats back to the mixed layer carrying outer-layer fluid with it. We were not able to see such details.

5. Principal experimental results

5.1. $t^{\frac{2}{11}}$ behaviour

In accordance with the predictions of (8) or (10), plots of D *vs.* $t^{\frac{2}{11}}$ (e.g. figure 3) were made, and, as described in §3, the distance of the virtual origin from the free surface d_0 was determined from the behaviour at smaller times. The plots of $D_* = D - d_0$, i.e. the distance measured from the virtual origin *vs.* $t^{\frac{2}{11}}$, and $\log(D-d_0)$ *vs.* $\log t$, are shown in figures 5 and 6. Up to the 'breakpoint' almost all graphs showed more than 99 % correlation for a least-square fit. The slope of the graph of $\log(D-d_0)$ *vs.* $\log t$ was found to be $\frac{2}{11}$.

5.2. V_0 dependence†

Several experiments were performed with the nearly constant frequency of about 10.5 rad/s (i.e. an action of about 18.5 cm^2/s) with V_0 varying over the range 7–40 cm/s. As discussed earlier, graphs of D *vs.* $t^{\frac{2}{11}}$ were first plotted and the slope

† We define $V_0^2 = D_0 \Delta b_0$, where D_0 and Δb_0 are evaluated at a time before the grid begins to oscillate. At that time, $h = 0$.

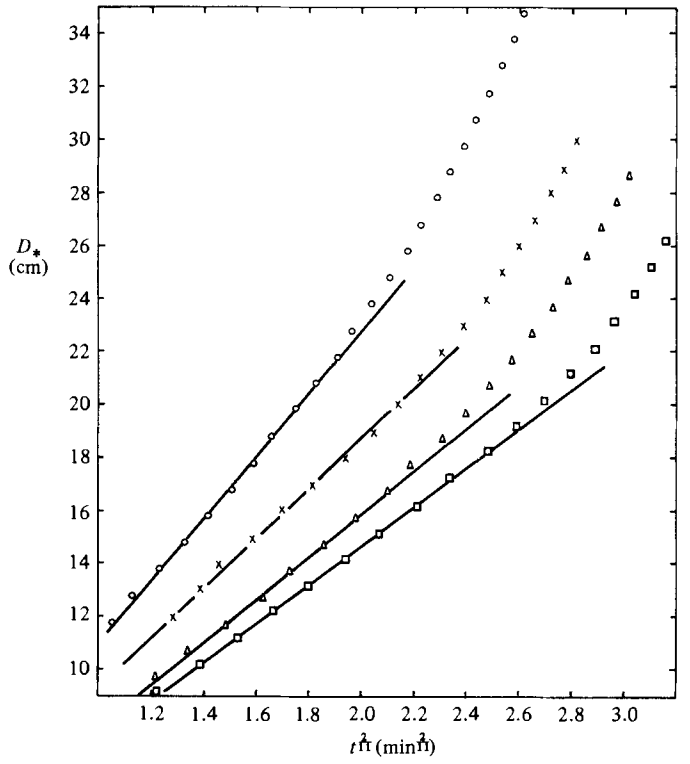

FIGURE 5. Graph of $D-d_0$ *vs*, $t^{\frac{2}{11}}$ at constant 'action' $K \approx 18.5$ cm^2/s. V_0 values in cm/s are □, 30.98; △, 24.68; ×, 20.95; ○, 15.24.

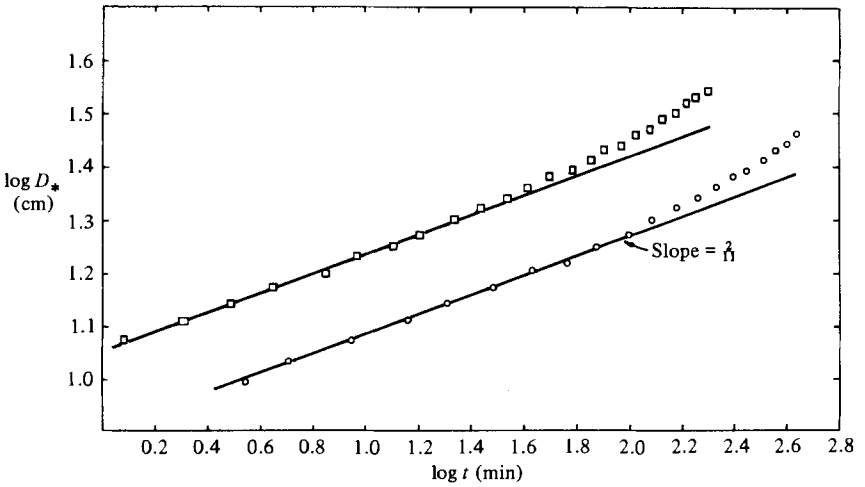

FIGURE 6. Graph of $\log(D-d_0)$ *vs*. $\log t$ for two experiments at constant 'action' $K = 18.5$ cm^2/s; V_0 values in cm/s are ○, 9.64; □, 7.27.

α was determined by a least-square fit. This slope was plotted against V_0 in a log–log plot, and the results are shown in figure 7. The best-fit curve for the experimental points were indistinguishable from a $-\frac{7}{11}$-graph and this supports (10), derived by Long (1978*b*), rather than (7), (8) or (9).

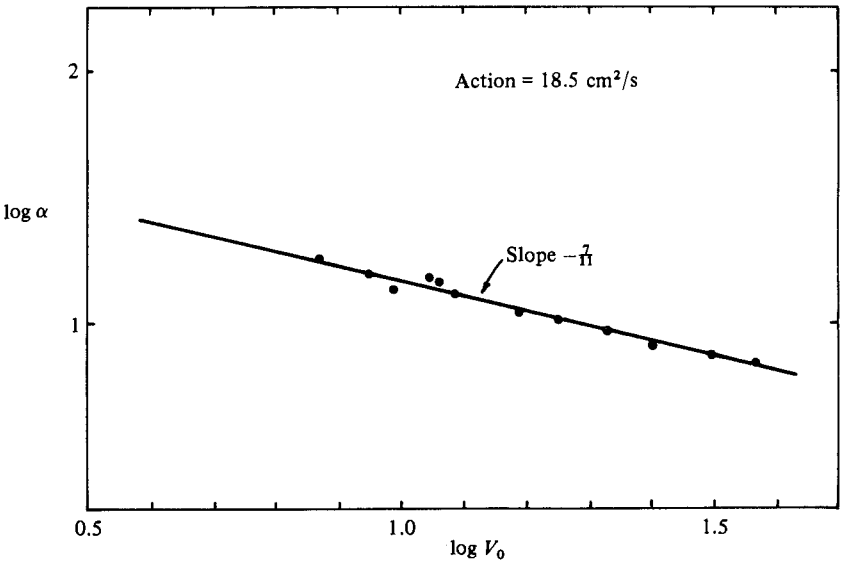

FIGURE 7. Graph of $\log \alpha$ *vs.* $\log V_0$ at constant 'action' $K = 18.5$ cm²/s.

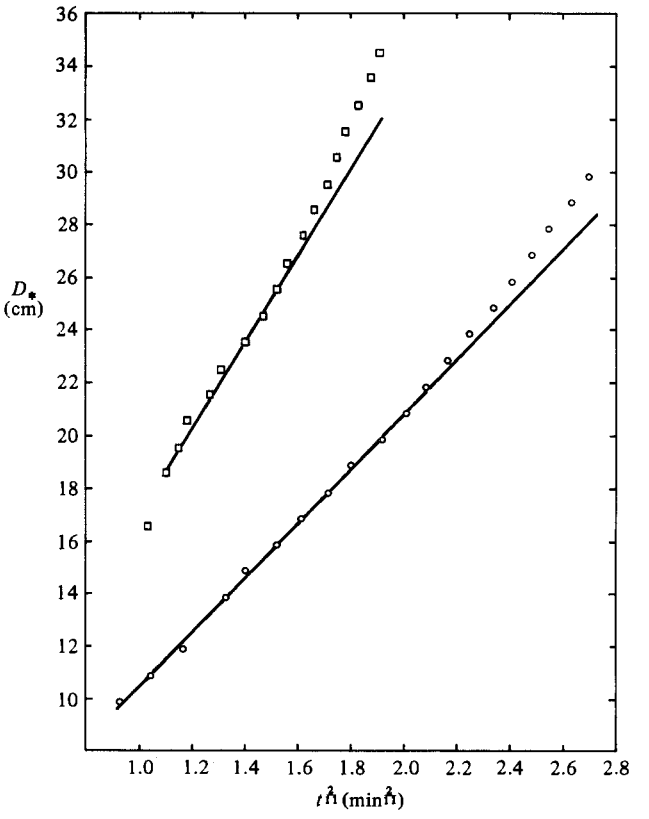

FIGURE 8. Graph of D_* *vs.* $t^{\frac{2}{11}}$ at constant $V_0 = 11.37$ cm/s: □, $K = 22.6$ cm²/s; ○, $K = 16.05$ cm²/s.

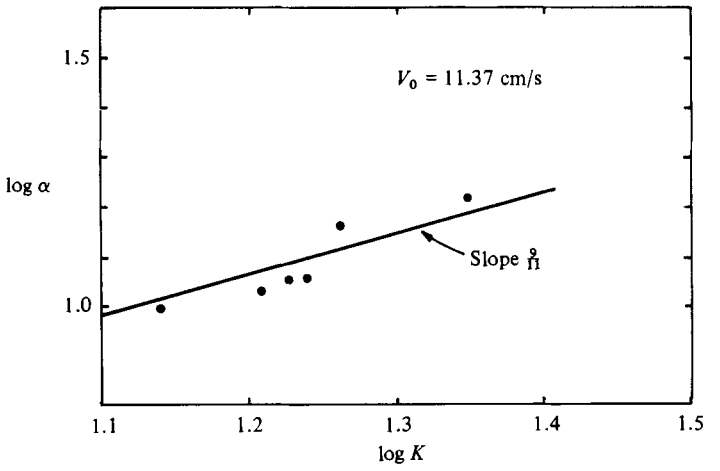

FIGURE 9. Graph of $\log\alpha$ *vs.* $\log K$ at constant $V_0 = 11.37$ cm/s.

5.3. *K-dependence*

To check the dependence of the deepening rate on the action K (or frequency ω), several experiments were conducted with a constant V_0 of 11.37 cm/s. The frequency was changed and the action was determined from the graph of figure 2. Only a small range of K of 14–18 cm^2/s was achieved owing to mechanical difficulties. Graphs of D *vs.* $t^{\frac{8}{11}}$ and D_* *vs.* $t^{\frac{8}{11}}$ were plotted (e.g. figure 8), and the resulting slope α was graphed in a log–log plot with K. Results are shown in figure 9, and this is also in good agreement with (10).

5.4. *Evaluation of universal constant* B_8

Accepting the validity of (10), we may evaluate the constant B_8 by two methods: (*a*) using the intercept of the $\log\alpha$ *vs.* $\log V_0$ graph (i.e. figure 7), and (*b*) using the intercept of the $\log\alpha$ *vs.* $\log K$ graph (figure 9). These calculations yielded values of B_8 of 2.63 and 2.50 respectively. Of course, the constant of proportionality is valid only up to the 'breakpoint' as discussed above.

5.5. *Interfacial-layer thickness variation with depth*

The interfacial-layer thickness h was determined by the conductivity/depth data as in figure 10, and it was observed that a linear relation exists between h and D_* with the interfacial-layer thickness about 0.1 times the depth of the mixed layer measured from a virtual origin. Laser-beam observations on the shadowgraph also verify the linear relation between h and D_* (figure 11), but we see that h/D_*, estimated from the laser-beam technique, is approximately 0.15. Crapper & Linden (1974) have performed a similar study of h/D_*, and their results also show that the thickness of the interfacial layer is a linear function of the mixed-layer depth at high Ri. The reader should not confuse h with the amplitude δ_2 of the interfacial waves. According to Long's (1978*b*) theory, the former varies only with D_*, whereas the latter decreases with larger Ri.

5.6. *Entrainment coefficient vs. Richardson number behaviour*

One of the most common attempts in mixing experiments is to determine the relationship between the entrainment coefficient $E = u_e/u_*$ and the Richardson

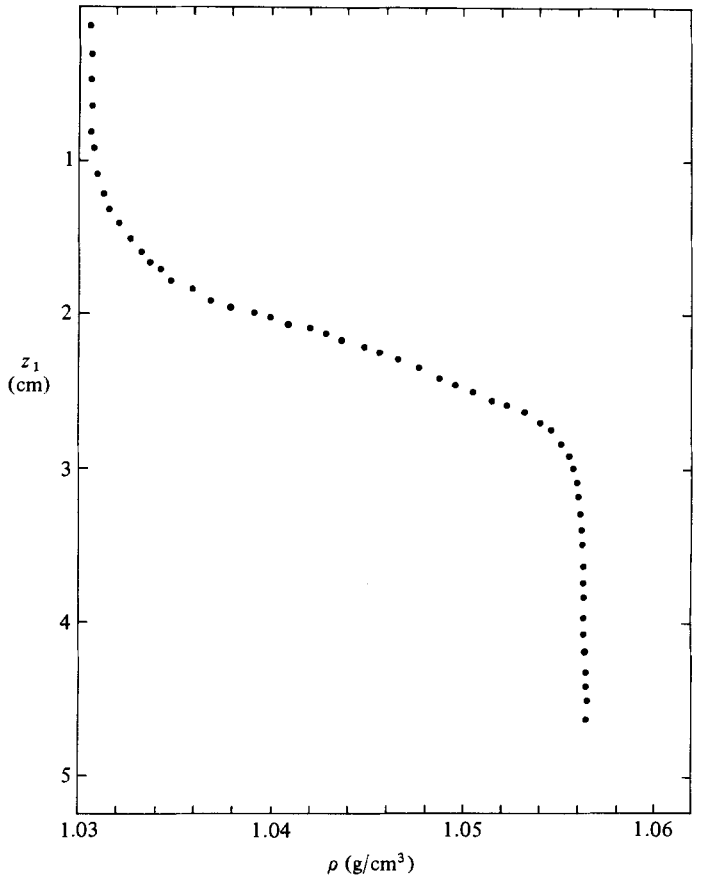

FIGURE 10. Typical profile of density. The depth z_1 is measured from an arbitrary origin.

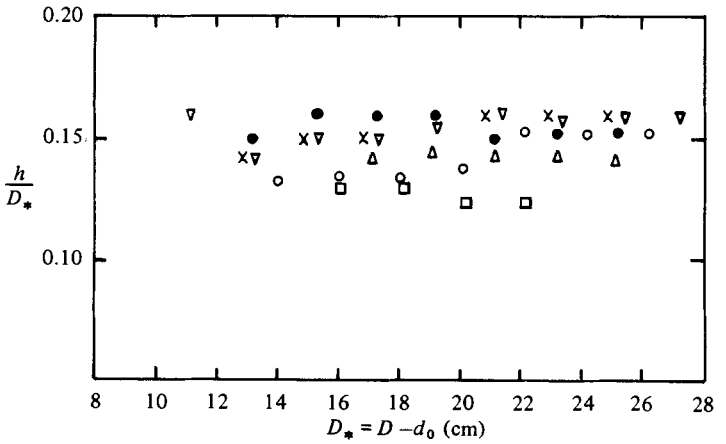

FIGURE 11. Variation of interfacial-layer thickness/mixed-layer thickness ratio with the depth of the mixed layer: □, $V_0 = 13.38$, $K = 18.40$; △, 15.22, 18.52; ●, 20.58, 18.52; ▽, 21.80, 18.40; ○, 23.09, 18.40; ×, 24.38, 18.40 (V_0 in cm/s, K in cm^2/s).

number Ri. Turner (1968), for example, carried out a series of experiments with oscillating grids. In these, the position of the interface was kept constant and the entrainment rate was determined using the rate of removal of water from the bottom layer, needed to keep the interfacial layer at a constant position. The results indicate that, for high Richardson numbers and with stratification by salt, $E \sim Ri^{-\frac{3}{2}}$. A similar relation was reported in the experiments of Hopfinger & Toly (1976). Long (1978*b*) derived (12), i.e. $E \sim Ri^{-\frac{1}{4}}$, as the entrainment law for the same experiments.

The Richardson number for the problem may be defined as $Ri = D_*^3 \Delta b / K^2$. Using the observation $h = \alpha_1 D_*$ and the fundamental constant for the problem given in Long (1978*b*),

$$\Delta b(D_* + \tfrac{1}{2}h) = V_0^2, \tag{13}$$

it is possible to define another form of a Richardson number

$$\widehat{Ri} = \frac{V_0^2 D_*^2}{K^2}, \tag{14}$$

where $\widehat{Ri} = (1 + \frac{1}{2}\alpha_1) Ri$.

A log–log plot of the entrainment coefficient *vs.* Richardson number is shown in figure 12, which reveals an excellent agreement with the prediction of (12) derived by Long (1978*b*), i.e. $E = \alpha_2 Ri^{-\frac{1}{4}}$ or $E = \alpha_3 \widehat{Ri}^{-\frac{1}{4}}$. The universal constants α_2 and α_3 may be found by the intercept of the line fitted to the $\log E$ *vs.* $\log \widehat{Ri}$ graph. This yields $\alpha_3 = 50$. Then, taking $\alpha_1 \approx 0.1$, we estimate $\alpha_2 = 46$. Notice that these values of α_2 and α_3, with the definition of 'action' $K = D_*^2/t$ in Dickinson & Long (1983), are very different from those estimated by Long (1978*b*), who used the definition $K_l = \sigma_u l$. Thus, using (2) with a proportionality constant 0.25 (average value of Hopfinger & Toly 1976) and (4) with $C_2 = 0.25$, it is possible to calculate $K_l = \sigma_u l$, and, based on this value, α_3 becomes 3.22×10^5 and α_2 becomes 2.96×10^5. This value of α_2 is consistent with Long (1978*b*), who predicted $\alpha_2 = 3.1 \times 10^5$. Notice also in figure 12 that the Hopfinger & Toly data (when expressed in terms of 'action' K) collapse well with our present data at higher $\widehat{Ri}$ and lend some additional support to the $Ri^{-\frac{1}{4}}$ behaviour.

5.7. *Depth–time behaviour after 'breakpoint'*

As we mentioned in §§3 and 4, after a certain depth, the slope of the D *vs.* $t^{\frac{2}{3}}$ curve increases, indicating a markedly increased entrainment rate (figures 3, 5 and 6). In view of the excellent agreement between the observed entrainment at smaller times (depths) and the theory (which assumes a horizontally infinite fluid), it is reasonable to suppose that the behaviour after 'breakpoint' is a wall effect, perhaps because the walls cause an increased vertical velocity due to flattening and this in turn leads to higher velocities tangent to the interface and so higher entrainment rates. Then the width W of the vessel enters the problem as a new parameter, i.e.

$$u_e = f(V_0, K, D_*, W). \tag{15}$$

Non-dimensionalization yields

$$E = \frac{u_e D_*}{K} = g\left(\widehat{Ri}, \frac{D_*}{W}\right). \tag{16}$$

In contrast with the observed collapse of the E *vs.* $\widehat{Ri}$ data for earlier times (figure 12), figure 13 shows the absence of collapse after the 'breakpoint'. Log–log plots of

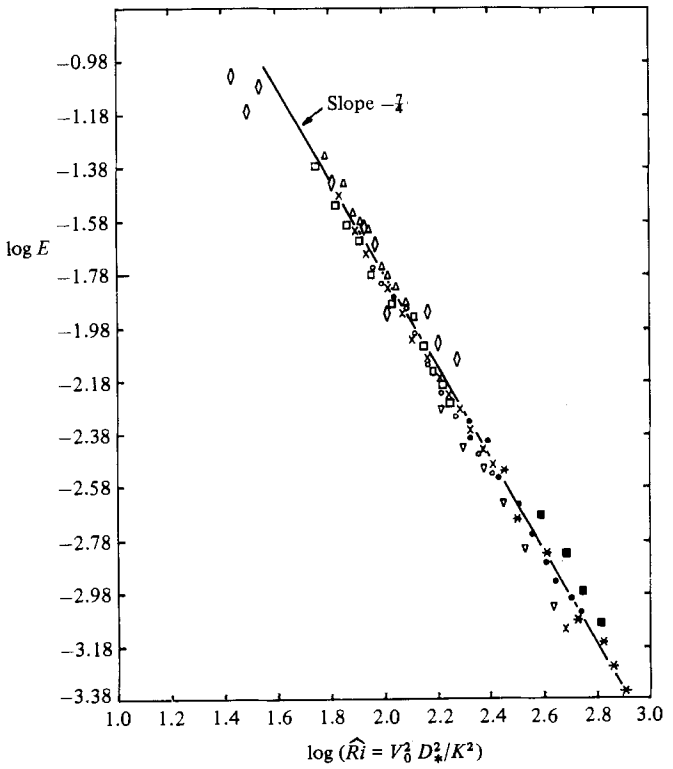

FIGURE 12. Graph of $\log E$ *vs.* $\log \widehat{Ri}$ for 8 different experimental runs: □, $V_0 = 8.81$, $K = 18.7$; ×, 9.64, 18.2; *, 17.72, 18.7; △, 15.24, 18.7; ●, 20.95, 18.2; ▽, 24.68, 18.7; ○, 30.98, 18.7; ■, 35.57, 18.2 (V_0 in cm/s, K in cm²/s). ◇, data of Hopfinger & Toly with $K = 46.23$ cm²/s.

E *vs.* D_*/W at constant Richardson number $\widehat{Ri}$ were made (not shown), and, in a search for collapse, the empirical behaviour $E \sim (D_*/W)^{1.39}$ was chosen. A plot was then made and the collapsed results are shown in figure 14. This figure suggests the behaviour

$$E \sim \widehat{Ri}^{-\frac{3}{2}} \left(\frac{D_*}{W}\right)^{1.39}. \tag{17}$$

We point out that this empirical relation does not lead to (12) in the asymptotic limit $D_*/W \to 0$, but this, perhaps, is not unexpected because the two regions have different dynamics.

5.8. *Variation of the position of the breakpoint*

A final observation is the dependence of the position of the breakpoint of figures 3, 5, 6 and 8 as discussed in §3. A plot of the occurrence of the breakpoint against the length $L_* = K/V_0$ is shown in figure 15. Since we came to the tentative conclusion that the breakpoint is a wall effect, dimensional analysis suggests the relation

$$D_{*b} = \frac{K}{V_0} f\left(\frac{K}{V_0 W}\right). \tag{18}$$

W, of course, is a constant length in this experiment, so that D_{*b} is a function only of the variable length $L_* = K/V_0$, as figure 15 perhaps indicates.

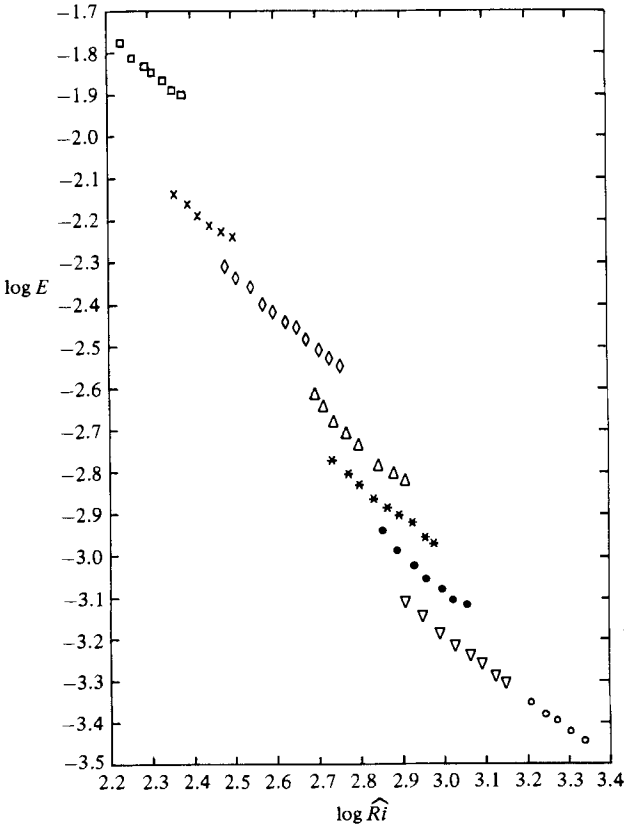

FIGURE 13. Graph of $\log E$ *vs.* $\log \widehat{Ri}$ after the 'breakpoint' for 8 different experimental runs. Symbols have the same meaning as figure 12, except ◇, $V_0 = 12.03$ cm/s, $K = 18.7$ cm²/s; □, 7.27 cm/s, 18.2 cm²/s.

The physical significance of L_* is of interest. If δ is the amplitude of the wave disturbances in the interfacial layer, equating potential and kinetic energies yields

$$\sigma_u^2 \sim \frac{\Delta b}{h}\delta^2, \tag{19}$$

where σ_u is the r.m.s. velocity of the eddies at the interface and h is the thickness of the interfacial layer. Using $h = \alpha_1 D_*$, where $\alpha_1 \approx 0.1$, we find

$$\Delta b = \frac{V_0^2}{D_*(1+\frac{1}{2}\alpha_1)}. \tag{20}$$

Then (19) and (20) and $\sigma_u \sim K/D_*$ yield

$$\delta \sim L_*, \tag{21}$$

indicating that L_* is a length proportional to the amplitude of the interfacial-wave disturbances caused by energy-containing eddies.

5.9. *Variation of interfacial-layer wave frequency with Ri*

As mentioned in §3 and as seen in figure 4, we recorded the conductivity fluctuations at various positions in the fluid. The large-amplitude fluctuations in the upper part

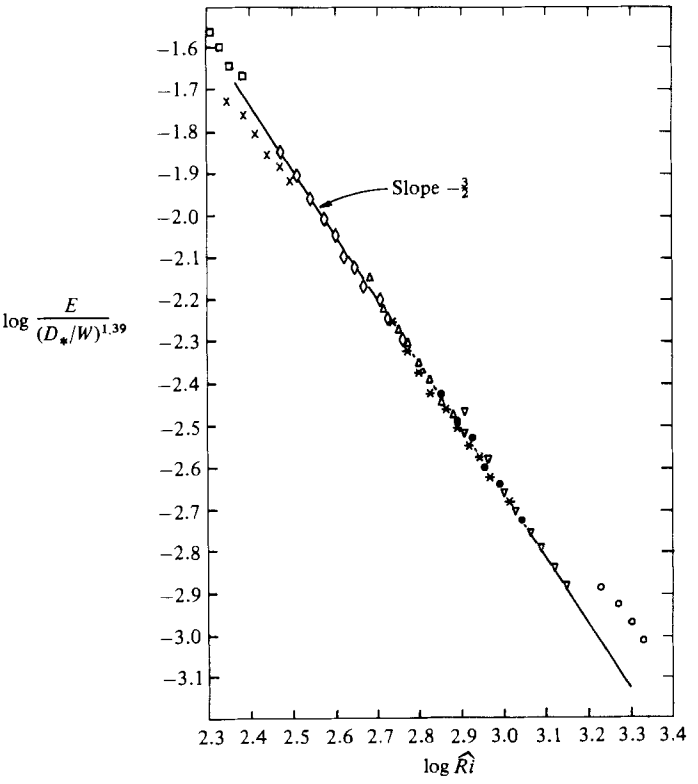

FIGURE 14. Graph of $\log[E/(D_*/W)^{1.39}]$ *vs.* $\log \widehat{Ri}$ after the 'breakpoint' for the same experiments as in figure 13.

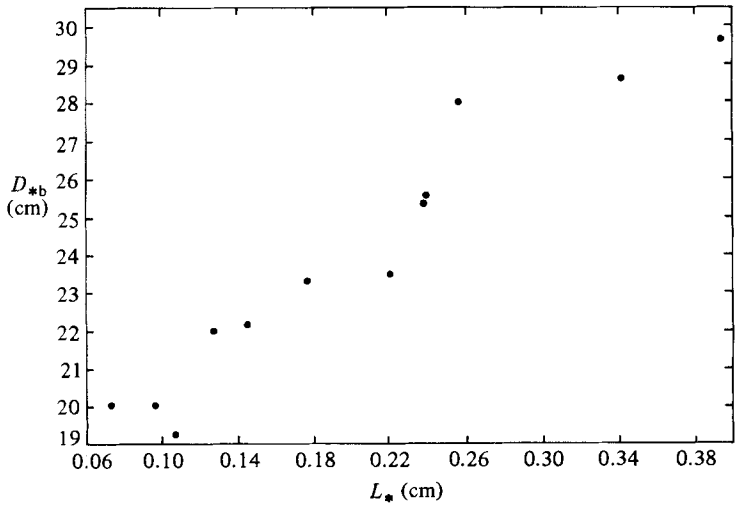

FIGURE 15. Variation of breakpoint D_{*b} (measured from the virtual origin) with the lengthscale $L = K/V_0$.

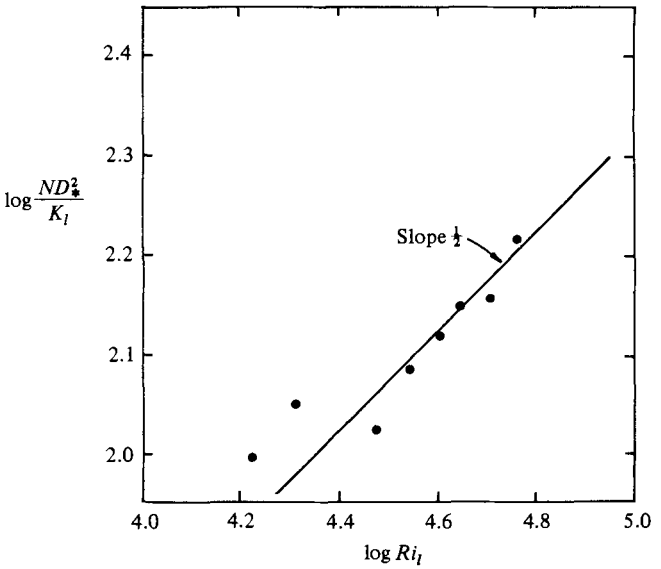

FIGURE 16. Graph of non-dimensional frequency of disturbances near the top of the interfacial layer *vs.* the Richardson number $Ri_l = D_*^3 \Delta b / K_l^2$.

of figure 4 are characteristic of the upper portion of the interfacial layer, and we analysed eight such records in order to compare measurements of the period of the large fluctuations with the theory of Long (1978*b*). The theory predicted

$$\frac{w_2}{K_l/D_*} = \alpha_4 Ri_l^{-\frac{1}{4}}, \tag{22}$$

$$\frac{\delta_2}{D_*} = \alpha_5 Ri_l^{-\frac{3}{4}}, \tag{23}$$

where w_2 and δ_2 are the characteristic velocity and lengthscales of the quasi-isotropic eddies just above the interface, $Ri_l = D_*^3 \Delta b / K_l^2$ is the Richardson number, and α_4, α_5 are universal constants estimated by Long (1978*b*) as $\alpha_4 = 31, \alpha_5 = 15.7$. According to the theory, these eddies cause the large interfacial disturbances, which therefore have the frequency $N = w_2/\delta_2$, or

$$\frac{ND_*^2}{K_l} = \frac{\alpha_4}{\alpha_5} Ri_l^{\frac{1}{4}}. \tag{24}$$

To compare with measurements and to be as objective as possible, we calculated the frequency of the zero-crossings of the conductivity signal for the large-amplitude fluctuations at the upper portion of the interfacial layer, and the result is shown in figure 16. The agreement is only fair. The line drawn in yields a value of $\alpha_4/\alpha_5 = 0.66$ compared with Long's estimate of 1.97.

6. Conclusions

The experimental results above show that turbulent entrainment in a two-fluid system generated by an oscillating grid can be well described by a theory of Long (1978*b*) in which the depth of the mixed layer, the thickness of the interfacial layer and the entrainment rate are given by (10), (11) and (12). After a certain depth, in

the vicinity of 28–34 cm from the top of the mixed layer, the entrainment laws tend to deviate from this theory; the deviation is due, possibly, to the entrapment of eddies between the walls, thus changing the entrainment mechanism.

Fruitful discussions with Professors O. M. Phillips, S. A. Kitaigorodskii and S. Corrsin are greatly appreciated. The authors wish to thank Andrew Pipino and Michael Steele for their support in carrying out the experiments. This research was supported by the National Science Foundation Grants ATM-7907026 and ATM-8210498 and the Office of Naval Research (Fluid Dynamics Division) Contract no. N00014-76-C-0184.

REFERENCES

BAINES, W. D. 1975 Entrainment by a plume or a jet at a density interface. *J. Fluid Mech.* **68**, 309.

BOUVARD, M. & DUMAS, H. 1967 Application de la méthode du fil chaud à la mesure de la turbulence dans l'eau. *Houille Blanche* **22**, 257.

BROWN, F. L. & ROSHKO, A. 1974 On density effects and large structure in turbulent mixing layers. *J. Fluid Mech.* **64**, 775.

CORRSIN, S. 1963 Turbulence: experimental methods. *Handbuch der Physik*, vol. VIII/2, *Strömungsmechanik*, II, p. 547. Springer.

CRAPPER, P. F. & LINDEN, P. F. 1974 The structure of turbulent density interfaces. *J. Fluid Mech.* **65**, 45.

CROMWELL, T., 1960 Pycnoclines created by mixing in an aquarium tank. *J. Mar. Res.* **18**, 73.

DEARDORFF, J. W. & WILLIS, G. E. 1982 Dependence of mixed layer entrainment on shear stress and velocity jump. *J. Fluid Mech.* **115**, 123.

DEARDORFF, J. W., WILLIS, G. E. & LILLY, D. K. 1969 Laboratory investigation of nonsteady penetrative convection. *J. Fluid Mech.* **35**, 7.

DEARDORFF, J. W., WILLIS, G. E. & STOCKTON, B. H. 1980 Laboratory studies of entrainment zone of a convective mixed layer. *J. Fluid Mech.* **100**, 41.

DICKINSON, S. C. 1980 Oscillating grid turbulence including effects of rotation. Ph.D. thesis, The Johns Hopkins University.

DICKINSON, S. C. & LONG, R. R. 1978 Laboratory study of the growth of a turbulent layer of fluid. *Phys. Fluids* **21**, 1698.

DICKINSON, S. C. & LONG, R. R. 1983 Oscillating grid turbulence including the effects of rotation. *J. Fluid Mech.* **126**, 315.

EKMAN, V. W. 1905 On the influence of the earth's rotation on ocean currents. *Ark. Mat. Astr. Fys.* **2** (11), 1.

ELLISON, T. H. & TURNER, J. S. 1959 Turbulent entrainment in stratified flows. *J. Fluid Mech.* **6**, 423.

FISHER, H., LIST, J., KOH, R., IMBERGER, J. & BROOKS, N. 1979 *Mixing in Inland and Coastal Waters*. Academic.

FOLSE, R. F., COX, T. P. & SCHEXNAYDER, K. R. 1981 Measurements of the growth of a turbulently mixed layer in a linearly stratified fluid. *Phys. Fluids* **24**, 396.

HOPFINGER, E. J. & LINDEN, P. F. 1982 Formation of thermocline in zero-mean-shear turbulence subjected to a stabilizing buoyancy flux. *J. Fluid Mech.* **114**, 157.

HOPFINGER, E. J. & TOLY, J.-A. 1976 Spatially decaying turbulence and its relation to mixing across density interfaces. *J. Fluid Mech.* **78**, 155.

HUNT, J. C. R. & GRAHAM, J. M. R. 1978 Free-stream turbulence near plane boundaries. *J. Fluid Mech.* **84**, 209.

IVEY, G. N. & CORCOS, G. M. 1982 Boundary mixing in a stratified fluid. *J. Fluid Mech.* **121**, 1.

KANTHA, L. H. & LONG, R. R. 1980 Turbulent mixing with stabilizing surface buoyancy flux. *Phys. Fluids* **23**, 2142.

KANTHA, L. H., PHILLIPS, O. M. & AZAD, R. S. 1977 On turbulent entrainment at a stable density interface. *J. Fluid Mech.* **79**, 753.

KATO, H. & PHILLIPS, O. M. 1969 On the penetration of a turbulent layer into a stratified fluid. *J. Fluid Mech.* **37**, 673.

KITAIGORODSKII, S. A. 1979 Review of the theories of wind-mixed layer deepening. *Marine Forecasting, Elsevier Oceanographic Ser.* **25**, 1.

KLINE, S. J. & MCCLINTOCK, F. A. 1953 Describing uncertainties in single sample experiments. *Mech. Engng* (January), p. 3.

LESHUK, J. P., ZAWORSKII, R. J., STYRIS, D. L. & HARLING, O. K. 1978 Solar pond stability experiments. *Solar Energy* **21**, 237.

LINDEN, P. F. 1973 The interaction of a vortex ring with a sharp density interface: a model for turbulent entrainment. *J. Fluid Mech.* **60**, 467.

LINDEN, P. F. 1975 The deepening of a mixed layer in a stratified fluid. *J. Fluid Mech.* **71**, 385.

LOFTQUIST, K. 1960 Flow and stress near an interface between stratified liquids. *Phys. Fluids* **3**, 158.

LONG, R. R. 1978*a* Theory of turbulence in a homogeneous fluid induced by an oscillating grid. *Phys. Fluids* **21**, 1887.

LONG, R. R. 1978*b* A theory of mixing in a stably stratified fluid. *J. Fluid Mech.* **84**, 113.

LONG, R. R. & KANTHA, L. H. 1979 The rise of a strong inversion caused by heating of the ground. In *Proc. 12th Symp. on Naval Hydrodynamics, Natl Acad. Sci.*, p. 585.

MCDOUGALL, T. J. 1979 Measurements of turbulence in a zero-mean-shear mixed layer. *J. Fluid Mech.* **94**, 409.

MOORE, M. J. & LONG, R. R. 1971 An experimental investigation of turbulent stratified shearing flow. *J. Fluid Mech.* **49**, 635.

PHILLIPS, O. M. 1976 *Dynamics of the Upper Ocean.* Cambridge University Press.

PIAT, J. F. & HOPFINGER, E. J. 1981 A boundary layer topped by a density interface. *J. Fluid Mech.* **113**, 411.

ROUSE, H. & DODU, J. 1955 Turbulent diffusion across a density discontinuity. *Houille Blanche* **10**, 522.

SCRANTON, D. R. & LINDBERG, W. R. 1982 An experimental study of entraining stress-driven, stratified flow in an annulus. Submitted to *Phys. Fluids.*

THOMPSON, S. M. 1969 Turbulent interfaces generated by an oscillating grid in a stably stratified fluid. Ph.D. thesis, University of Cambridge.

THOMPSON, S. M. & TURNER, J. S. 1975 Mixing across an interface due to turbulence generated by an oscillating grid. *J. Fluid Mech.* **67**, 349.

THORPE, S. A. 1973 Turbulence in stably stratified fluids: a review of laboratory experiments. *Boundary-Layer Met.* **5**, 95.

TURNER, J. S. 1968 The influence of molecular diffusivity on turbulent entrainment across a density interface. *J. Fluid Mech.* **33**, 639.

TURNER, J. S. 1973 *Buoyancy Effects in Fluids.* Cambridge University Press.

TURNER, J. S. & KRAUS, E. B. 1967 A one-dimensional model of the seasonal thermocline: I. A laboratory experiment and its interpretation. *Tellus* **19**, 88.

WOLANSKI, E. J. 1972 Turbulent entrainment across stable density-stratified liquids and suspensions. Ph.D. thesis, The Johns Hopkins University.

WOLANSKI, E. J. & BRUSH, L. M. 1975 Turbulent entrainment across stable density step structures. *Tellus* **27**, 259.

WU, J. 1973 Wind-induced turbulent entrainment across a stable density interface. *J. Fluid Mech.* **61**, 275.